Experimental study of electrostatic precipitator performance and comparison with existing theoretical prediction models

S.H. Kim, K.W. Lee*

Kwangju Institute of Science and Technology, Department of Environmental Science and Engineering, 1 Oryong-dong, Puk-gu, Kwangju 500-712, South Korea

Abstract

A laboratory-scale single-stage electrostatic precipitator (ESP) was designed, built and operated in a wind tunnel. As a first step, a series of experiments were conducted to seek the operating conditions for increasing the particle collection efficiency by varying basic operating parameters including the wire-to-plate spacing, the wire radius, the air velocity, the turbulence intensity and the applied voltage. As the diameter of the discharging wires and the wire-to-plate spacing are set smaller, the higher collection efficiency has been obtained. In the single-stage multiwire ESP, there exists an optimum wire-to-wire spacing which provides maximum particle collection efficiency. As the air velocity increases, the particle collection efficiency decreases. The turbulent flow is found to play an important role in the relatively low electric field region. In the high electric field region, however, particles can be deposited on the collection plates readily regardless of the turbulence intensity. The experimental results were compared with existing theories and Zhibin and Guoquan (Aerosol Sci. Technol. 20 (1994) 169–176) was identified to be the best model for predicting the ESP performance. As the second step, the influence of particle contamination at the discharging electrode and at the collection plates were experimentally measured. The methods were sought for keeping the high collection efficiency of ESP over elapsed time by varying the magnitude of rapping acceleration, the time interval between raps, the types of rapping system (hammer/vibrator) and the particle re-entrainment. The rapping efficiency and the particle re-entrainment were increased with increasing magnitude of rapping acceleration and time interval between raps. However, when the thickness of deposited fly ash layer is sufficiently high, the concentration of re-entrained particles starts decreasing abruptly due to the agglomeration force which can interact among

---

*Corresponding author. Tel.: + 82-62-970-2438; fax: + 82-62-970-2434.

E-mail address: lee@kjist.ac.kr (K.W. Lee)

deposited particles. The combined rapping system is found more effective for removing deposited particles than the hammer rapping system only. © 1999 Elsevier Science B.V. All rights reserved.

1. Introduction

Electrostatic precipitators (ESPs) are one of the most commonly employed particulate control devices for collecting fly ash emissions from boilers, incinerators and from many other industrial processes. They can operate in a wide range of gas temperatures achieving high particle collection efficiency compared with mechanical devices such as cyclones and bag filters. The electrostatic precipitation process involves several complicated and interrelated physical mechanisms: creation of a non-uniform electric field and ionic current in a corona discharge, ionic and electronic charging of particles moving in combined electro- and hydrodynamic fields, and turbulent transport of charged particles to a collection surface.

Generally, the collection efficiency of ESP decreases as the discharging electrode and collection plates are contaminated with particulates. Thus, a rapping system is needed for removing the collected particulates periodically. While there have been numerous theoretical and experimental studies on particle collection characteristics of electrostatic precipitators, a relatively small number of the studies addressed the effects of particle accumulation both at the discharging electrodes and at the collection plates. Both phenomena are known to influence adversely the performance of electrostatic precipitators. Many researchers, such as Deutsch [1], Cooperman [2], Leonard et al. [3], Khim et al. [4], Zhibin and Guoquan [5], and Kallio and Stock [6], conducted particle collection measurements of ESP. However, they concentrated mostly on the effects of both turbulent mixing and secondary wind in multiwire single-stage electrostatic precipitators. Specifically, Cooperman [2] considered re-entrainment and longitudinal turbulent mixing effects, Leonard et al. [3] the finite diffusivity, and Zhibin and Guoquan [7] the non-uniform air velocity profile. Among them, only Zhibin and Guoquan [7] measured the collection efficiency of a single-stage ESP covering a wide particle size range. Even though their experimental data are considered to be practical and useful, their experimental conditions were not identified clearly.

In the present study, well-defined collection efficiency data for an ESP are presented covering the particle size range of 0.1–100 μm. The particles used in the present study came from the Bo-Ryung power plant in Korea. In addition, the ESP performance was evaluated in terms of optimum operating conditions. Finally, the optimum rapping conditions were sought under which the rapping efficiency increases and the particle re-entrainment decreases.

2. Review of theoretical models

2.1. Particle charging

Fig. 1 shows the laboratory-scale electrostatic precipitator. The particle charging system consists of discharge wires with diameter (D_w) and two grounded parallel plates of length (L). A high negative voltage (V_w) is applied to the corona discharge wires, and suspended particles of diameter (d_p) flow with air between the plates at a velocity (U) in the y-direction. In the whole range of particle sizes, both field charging and diffusion charging mechanisms contribute to significant charges [8,9]. In these theoretical analyses, it is nearly correct to sum the rates of charging from the two mechanisms and then solve for the particle charging as follows:

$$\frac{dq_p}{dt} = \frac{q_s}{\tau}\left(1 - \frac{q}{q_s}\right)^2 + \frac{d_p^2 e N_0}{4}\sqrt{\frac{8kT\pi}{m}}\exp\left(-\frac{2qe}{d_p kT}\right) \tag{1}$$

where q_p is the particle charge, q_s is the saturation charge, N_0 is the average number of molecules per unit volume, e is the electronic charge ($= 1.6 \times 10^{-19}$ C), b is the ion mobility ($= 1.4 \times 10^{-4}$ m^2/V s), ε_0 is the permittivity of free space ($= 8.85 \times 10^{-12}$ F/m), d_p is the diameter of particle, k is the Boltzmann constant ($= 1.38 \times 10^{-23}$ J/K), T is the absolute temperature ($= 293$ K), m is the mass of a particle ($= (\pi/6)d_p^3\rho_p$), and ρ_p is the particle density ($= 2.25 \times 10^3$ kg/m^3).

2.2. Theoretical models of particle collection efficiency

Theoretical models of ESPs were provided by Deutsch [1], Cooperman [2], Leonard et al. [3], Zhibin and Guoquan [7] and others. The Deutsch model for
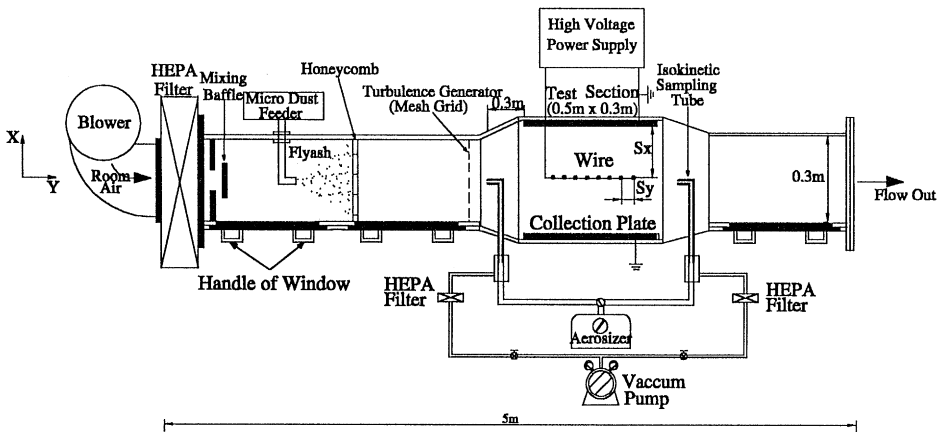

Fig. 1. Schematic diagram of the wind tunnel for the eight wired single-stage ESP performance test.

calculating the particle collection in an ESP assumes complete mixing by turbulent flow and thereby uniform concentration profiles. In order to improve the drastic assumption of infinite diffusivity in the Deutsch model, many researchers tried to develop finite diffusivity models by dealing with the convective-diffusion equation with various boundary conditions.

Cooperman [2] developed a theory which modifies the Deutsch model to account for the effects of turbulence and particle turbulent diffusion. The major limitations of the Cooperman model lie absence of a general method to estimate the re-entrainment factor and the particle diffusivity. Leonard et al. [3] developed a more complicated two-dimensional model using the method of the separation of variables from the convective-diffusion equation. He assumed uniformity of velocity components of charged particles and particle diffusivity. This assumption fails to adequately describe the particle diffusivity near the collection plates, where it is governed mainly by the molecular transport and, therefore, the diffusivity near the wall is significantly lower than the diffusivity in the turbulent core. Zhibin and Guoquan [7] suggested a new model for the single-stage ESP which takes into account the effect of turbulence mixing by electric wind. Predicted collection efficiencies of the above theoretical models are summarized as follows:

$$\eta_{De} = 1 - \exp(-De), \tag{2}$$

$$\eta_{Coo} = 1 - \exp\left[\frac{UL}{2D} - \sqrt{\left\{\left(\frac{UL}{2D}\right)^2 + (1-R)Pe\left(\frac{L}{W}\right)^2\right\}}\right], \tag{3}$$

$$\eta_{Leo} = 1 - \int_0^1 P\left(\frac{\xi - De}{\sqrt{2De/Pe}}\right)d\xi, \tag{4}$$

$$\eta_{Zhi} = 1 - \sqrt{\frac{Pe}{4\pi De}}\int_0^1 \exp\left[-\frac{Pe}{4De}(\xi - De)^2\right]d\xi, \tag{5}$$

where V_t is the migration velocity $(= q_p E C_c / 3\pi\mu d_p)$, C_c is the slip correction factor $(= 1 + (2/Pd_p)[6.32 + 2.01\exp(-0.1095 Pd_p)])$, P is the absolute pressure $(= 76\text{ cm Hg})$, E is the electric field intensity $(= V_w/W)$, W is the width of wire-to-plate, De is the Deutsch number $(= V_t L/UW)$, Pe is the electric Peclet number $(= V_t W/D_p)$, D_p is the particle diffusivity, and $P(z)$ in Eq. (4) is the Gaussian probability distribution function given by

$$P(z) = \frac{1}{\sqrt{2\pi}}\int_{-\infty}^{z}\exp\left(-\frac{B^2}{2}\right)dB. \tag{6}$$

In order to evaluate the particle diffusivity for the calculation of De and Pe, the flow is assumed to be a fully developed turbulent channel flow. The related physical quantities are specified like below [10]

$$\frac{1}{f^{1/2}} = -1.8\log_{10}\left(\frac{6.9}{Re}\right), \quad U_\tau = \sqrt{\frac{fU^2}{8}},$$

$$D_t = 0.12 U_\tau W, \quad D_B = \frac{kTC_c}{3\pi\mu d_p}, \quad D_p = D_t + D_B \tag{7}$$
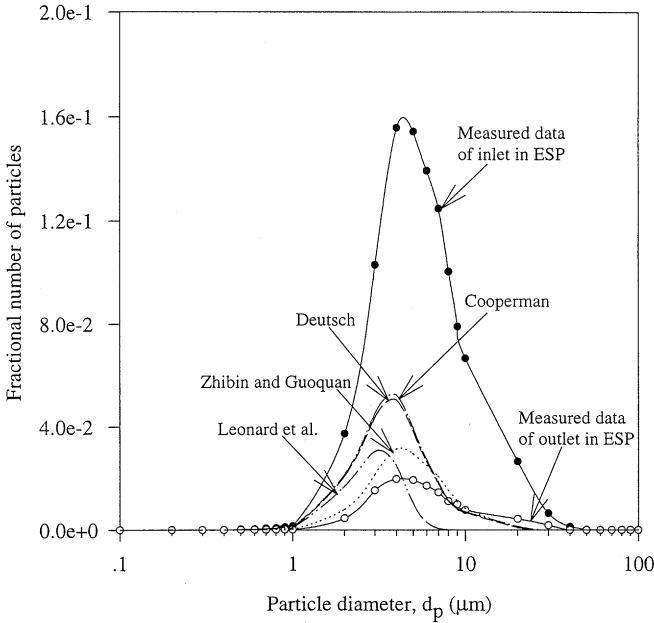
Fig. 2. Comparison of measured fractional number of particles with existing theoretical predictions. Experimental conditions: $D_w = 1$ mm, $V_w = 50$ kV, $S_x = 150$ mm, $S_y = 37.5$ mm, $U = 1$ m/s, $T_u = 12\%$.

where f is the friction factor, Re is the Reynolds number ($= 2UW/v$), U_τ is the friction velocity, D_t is the turbulent diffusivity, and D_B is the Brownian diffusivity.

With the measured data of fractional number of particles at the inlet of the single-stage ESP, measured fractional number of particles at the outlet of the single-stage ESP was compared with calculated results of each theoretical prediction model as shown in Fig. 2. The grade efficiency is computed over the particle size range 0.1–100 μm, and then integrated the grade efficiency to obtain the overall mass efficiency, where the particle size distribution function is assumed to be lognormal. The size distribution of most polydisperse aerosols is found very close to the lognormal distribution. Thus, this assumption is quite reasonable. The lognormal particle size distribution function is given by Herdan [11]:

$$f(d) = \frac{1}{d \ln \sigma_g (2\pi)^{0.5}} \exp\left[-\frac{(\ln d - \ln d_g)^2}{2 \ln^2 \sigma_g} \right] \tag{8}$$

where $\int_0^\infty f(d)\mathrm{d}d = 1$, the geometric mean diameter $d_g = 5.03$ μm and the geometric standard deviation $\sigma_g = 1.73$ from the measured data. The fraction number of each particle size at the outlet of ESP can be described by this particle size distribution function. Finally, the theoretical overall collection efficiency is calculated for comparison with the experimental results.

3. Experimental procedure

The experimental apparatus used in this study consisted of six components: an aerosol generation system, a wind tunnel, a laboratory-scale ESP, a rapping system, an aerosol sampling system, and a particle concentration measurement system. The ESP was 30 mm $(W) \times 500$ mm $(H) \times 750$ mm (L) in size and was equipped with eight discharge wires. The schematic diagram of the ESP is shown in Fig. 1. The basic operating conditions of the ESP and the parameters used are shown in Table 1. The single-lane wind tunnel was made of plexiglas and operated at the ambient temperature. It can provide air velocities ranging from 0.1 to 6 m/s. A thermo-anemometer (Model 8525, Alnor Instrument Company) was used to measure the air velocity. The air filtered with a high efficiency particulate filter (HEPA) was supplied with a turbulence intensity of about 12% and at a fixed mean velocity of 1 m/s. The fly ash particles which came from the Bo-Ryung electric power plant in Korea were dispersed using a microdust feeder (Model MF-2, Sibata Scientific Technology Ltd.). The fly ash was analyzed using chemical, physical and electrical methods and the analysis results are shown in Table 2. The microdust feeder utilizes a variable-speed turntable to transport fly ash at a constant rate to the test section in the wind tunnel. The laboratory-scale single-stage ESP described previously was installed in the test section as shown in Fig. 1. For aerosol sampling, an isokinetic sampling tube was used to measure the concentration and the size distribution of the fly ash particles. The measuring points were positioned at the center of the cross-sectional area of the wind tunnel. Measurements of the particle concentrations upstream and downstream were made by Aerosizer (Model Mach II and LD, API) which is capable of measuring individually the size of particles in the range of 0.2–200 μm regardless of the particle shapes. Finally, the overall collection efficiency, η_{exp}, was evaluated with the mass loading of the particles measured at inlet and outlet of the ESP:

$$\eta_{exp} = \frac{[(m)_{inlet} - (m)_{outlet}]}{(m)_{inlet}}, \tag{9}$$

Table 1
The dimensions and operating conditions for the present eight wire single-stage ESP

Dimensions and operating conditions	Values
Diameter of discharge wire, D_w (mm)	1, 2, 3, 4
Wire-to-plate spacing, S_x (mm)	50–200
Wire-to-wire spacing, S_y (mm)	12.5–50
Length of collection plate, L (m)	0.75
Height of collection plate, H (m)	0.3
Air flow velocity, U (m/s)	0.8–2.5
Applied voltage on wires, V_w (kV)	10–70
Turbulence intensity, T_u (%)	12, 15, 18
Air temperature, T (K)	293
Air pressure, P (atm)	1

Table 2
Results of chemical, physical, and electrical analysis of fly ash

Classification	Values
Chemcial components of fly ash	SiO_2 (46.47 wt%)
	Al_2O_3 (24.48 wt%)
	Fe_2O_3 (15.28 wt%)
	CaO (4.06 wt%)
	MgO (1.56 wt%)
	Na_2O (0.35 wt%)
	K_2O (1.17 wt%)
	SO_3 (4.20 wt%)
	TiO_2 (1.18 wt%)
Measurement of particle size distribution	GMD 5.03 m
	GSD 1.73
	$d_p \leqslant 4.23$ µm
	$d_p > 4.23$ µm
Electrical resistivity	4.3×10^9 (Ω m)

where $(m)_{inlet}$ is the mass loading of particles at the ESP inlet. $(m)_{outlet}$ is the mass loading of particles at the ESP outlet.

Presently, two philosophies are prevalent with regard to removal and transfer of the particulate from the collection plates. One approach is to rap periodically and to provide maximum rapping acceleration of in-plane vibration to the collection plates during each rap in an attempt to minimize the thickness of the residual dust layer. The other approach is to vary the intensity and frequency of rapping in order to minimize the quantity of material re-entrained. Although rapping is an important procedure for operating electrostatic precipitators, a relatively small number of studies addressed the effects of rapping and particle re-entrainment [12–16].

In this study, a rapping system was designed that consisted of a hammer and a vibrator. The optimum operating conditions for rapping were sought. Particle re-entrainment phenomenon was also studied at the same time. Accelerations of the hammer, the vibrator, and the collection plates were measured using a dynamic signal analyzer (Model 35670A, Hewlet Packard) and an accelerometer (Model 353B16, 353B34, Hewlet Packard). The impacting magnitude of the hammer was controlled by changing the angle of the handle of the hammer. The magnitude of vibration was controlled with a remote controller.

4. ESP performance under various operating conditions

As the first step, the optimum operating conditions for the ESP were sought by varying the design and operating parameters such as the wire-to-plate spacing, the wire-to-wire spacing, the air flow velocity, the turbulence intensity, and the diameter
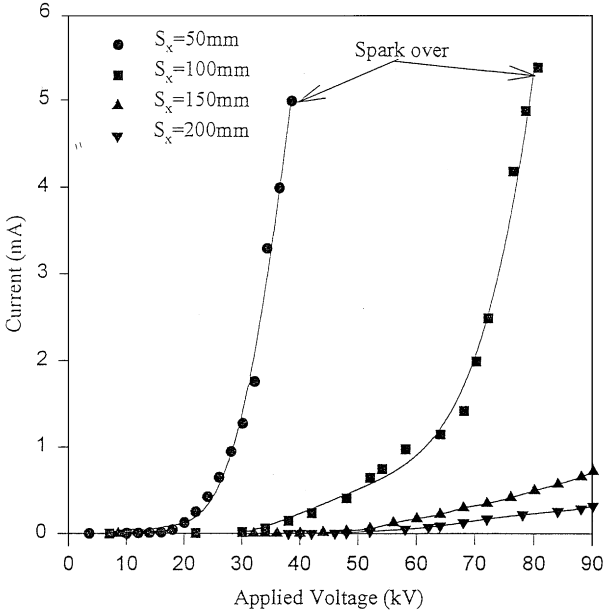
Fig. 3. Current–voltage characteristics in eight wire single-stage ESP. Experimental conditions: $D_w = 2$ mm, $S_y = 25$ mm, $U = 1$ m/s, $T_u = 12\%$.

of discharge wires. Before operating the ESP, corona current–voltage characteristics were measured for evaluating the electrical charge of loaded particles. While the high voltage was applied to the discharge electrode, the current was measured at the collection plates. For supplying high negative voltage, a DC power supply was used. One of the measured data is shown in Fig. 3. As the wire-to-plate spacing is decreased, the corona onset voltage is seen to decrease. The magnitude of the current changes greatly at a small wire-to-plate spacing even though applied voltage is small. Because the gas flow field is changed by increased movement of gas ions which is accelerated by the corona discharge. As the applied voltage increases more, sparkover which can change electric field occurs due to the unbalanced space charge density of local area in the present ESP. When the wire-to-plate spacing was increased, the collection efficiency decreased as shown in Fig. 4. In the given experimental conditions, Deutsch [1], Cooperman [2], and Zhibin and Guoquan [7] models are in a relatively good agreement with the experimental data in the wire-to-plate spacing range of 0.1–0.15 m. However, as the wire-to-plate spacing becomes larger than 0.1 m, Deutsch [1] and Cooperman [2] models underestimate the collection efficiency of ESP about 60% lower as shown in Fig. 5. The theory of Leonard et al. [3] overestimates the collection efficiency. Because it is becoming common to develop a wide-pitch ESP, the wire-to-plate distance was set at a fixed value, $S_x = 150$ mm in subsequent experiments. The discharging electrode was designed such that the wire-to-wire spacing can be varied from 12.5 to 50 mm. Fig. 6 shows that the wire-to-wire spacing
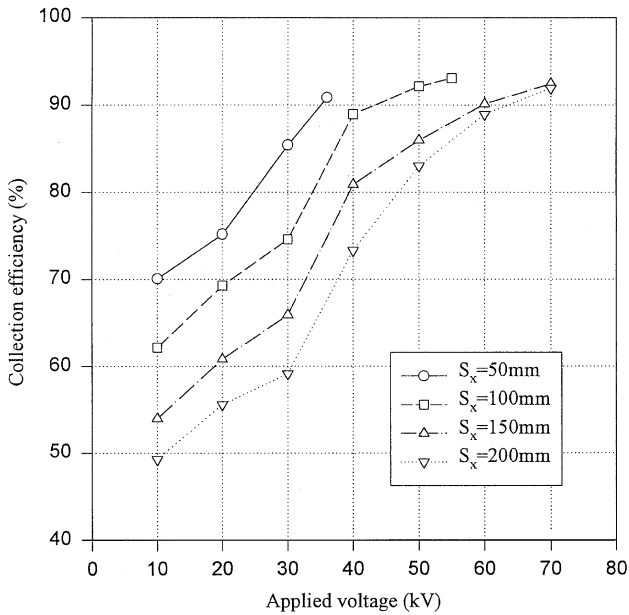
Fig. 4. Effect of wire-plate spacing on applied voltage and collection efficiency characteristics in single-stage ESP. Experimental conditions: $D_w = 2$ mm, $S_y = 25$ mm, $U = 1$ m/s, $T_u = 12\%$.
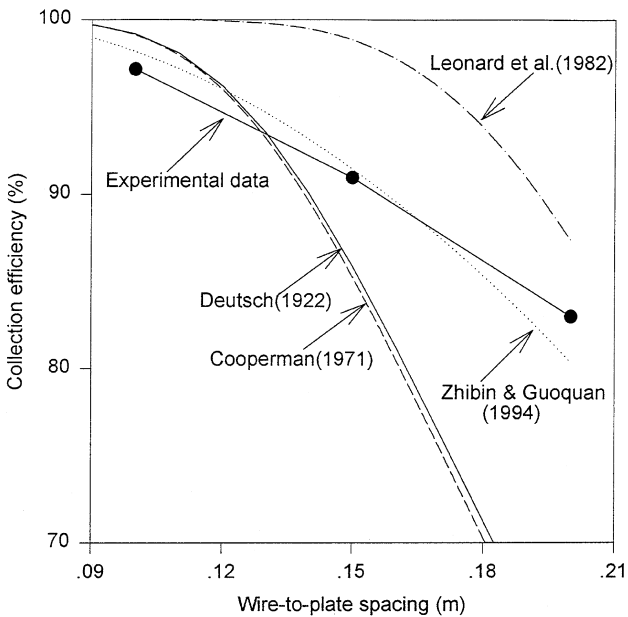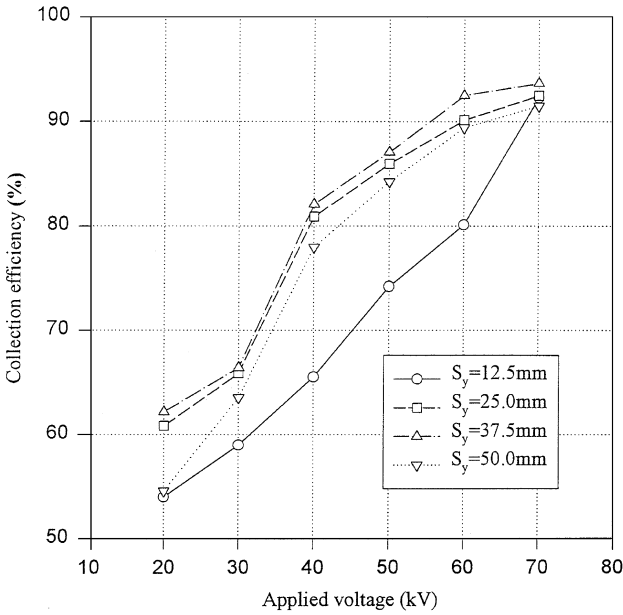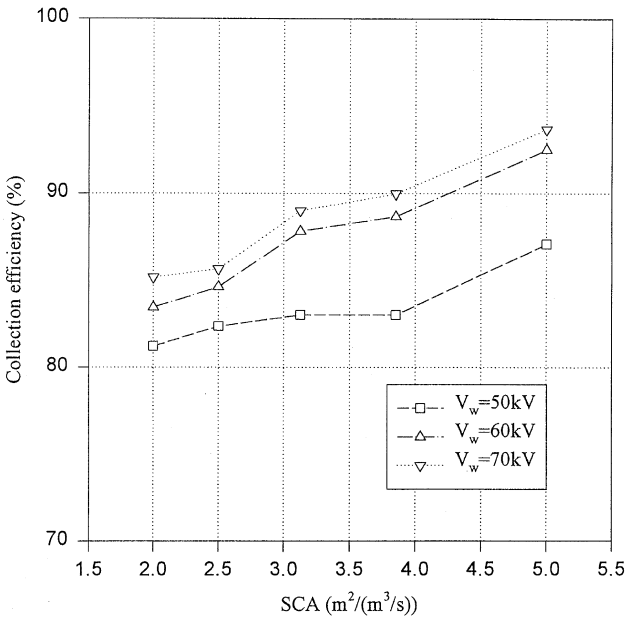

Fig. 5. Collection efficiency with various wire-to-plate spacing in single-stage ESP. Experimental conditions: $D_w = 2$ mm, $V_w = 50$ kV, $S_y = 25$ mm, $U = 1$ m/s, $T_u = 12\%$.

Fig. 6. Effect of wire-to-wire spacing and applied voltage on collection efficiency characteristics in single-stage ESP. Experimental conditions: $D_w = 2$ mm, $S_x = 150$ mm, $U = 1$ m/s, $T_u = 12\%$.

Fig. 7. Effect of applied voltage and SCA on collection efficiency characteristics in single-stage ESP. Experimental conditions: $D_w = 2$ mm, $S_x = 150$ mm, $S_y = 37.5$ mm, $T_u = 12\%$.
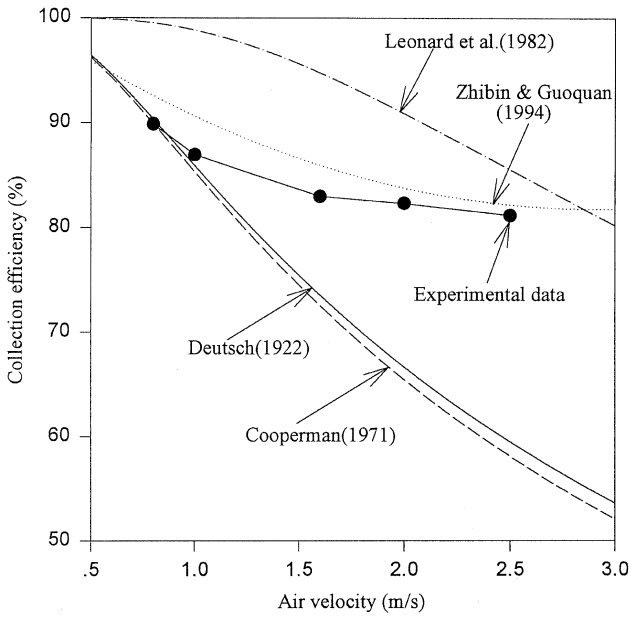
Fig. 8. Comparison of the total efficiency with the various velocities in single-stage ESP. Experimental conditions: $D_w = 2$ mm, $V_w = 50$ kV, $S_x = 150$ mm, $S_y = 37.5$ mm, $T_u = 12\%$.
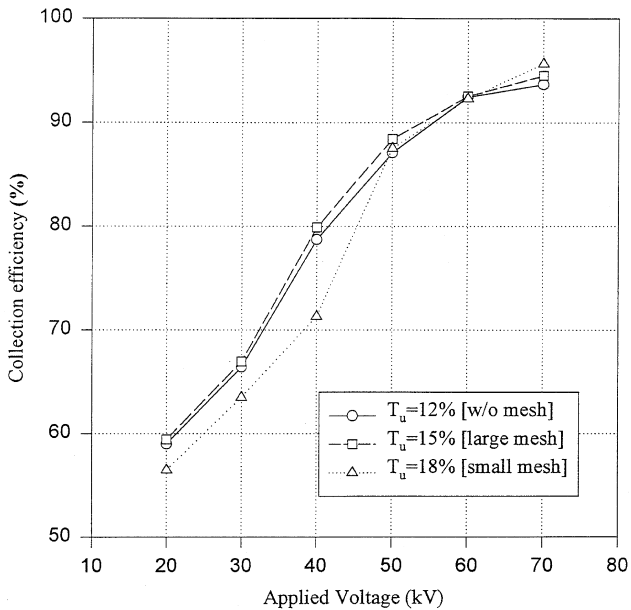

Fig. 9. Effects of turbulence intensity on applied voltage and collection efficiency characteristics in single-stage ESP. Experimental conditions: $D_w = 2$ mm, $S_x = 150$ mm, $S_y = 37.5$ mm, $U = 1$ m/s.

has significant effects on the ESP performance. In a given eight wire ESP, the wire-to-wire spacing was maintained at a fixed value, $S_y = 37.5$ mm where the collection efficiency is maximum. The specific collection are (SCA) defined as the ratio of the total collection area to the total gas volume flow rate is an important parameter that characterizes the performance of ESP. In this experiment, the total collection area of the plates was fixed. Thus, the SCA value was changed by varying the flow velocity (1, 1.3, 1.6, 2 and 2.5 m/s). As the flow velocity is increased, the SCA value becomes small and the collection efficiency of ESP decreases as shown in Fig. 7. The experimental data of the single-stage ESP were also compared with theoretical prediction models as shown in Fig. 8. It is observed that the Zhibin and Guoquan model is in a good agreement with the experimental data. The particles pass through a turbulence producing square mesh grid before entering an ESP. The turbulent flow field can be characterized by measuring both the mean velocity profile $U(x, y)$ and the streamwise root mean square turbulent velocity $u_{r.m.s.}(x, y)$. Here, the velocity in the x-direction can be ignored because it is so small compared with the velocity in the y-direction. Two types of mesh grids were designed. They were large mesh ($M = 12$ mm, $d_w = 1.2$ mm) and small mesh ($M = 6$ mm, $d_w = 0.6$ mm) where M is the mesh size and d_w is the diameter of mesh wires. These meshes were installed in front of the ESP test section providing different turbulence intensities. The measured turbulence intensity (T_u) was 12% without the mesh, 15% with large mesh and 18% with the small mesh, respectively. As seen in Fig. 9, the collection efficiency could greatly increase as
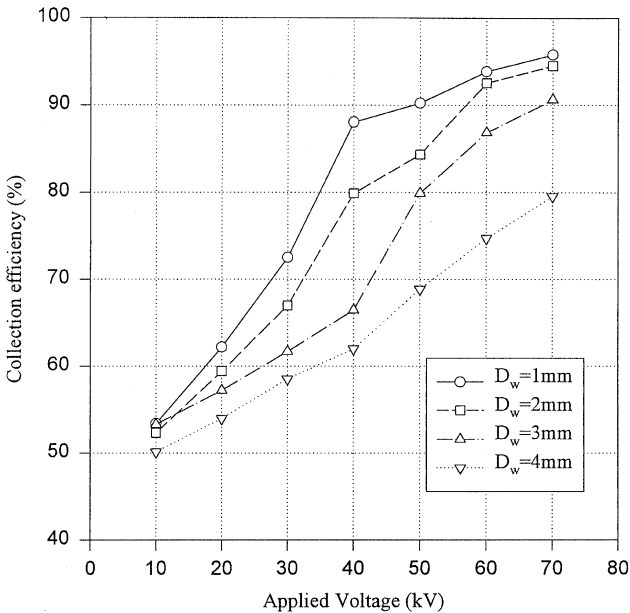

Fig. 10. Effect of wire diameter on applied voltage and collection efficiency characteristics in single-stage ESP. Experimental conditions: $S_x = 150$ mm, $S_y = 37.5$ mm, $U = 1$ m/s, $T_u = 12$%.
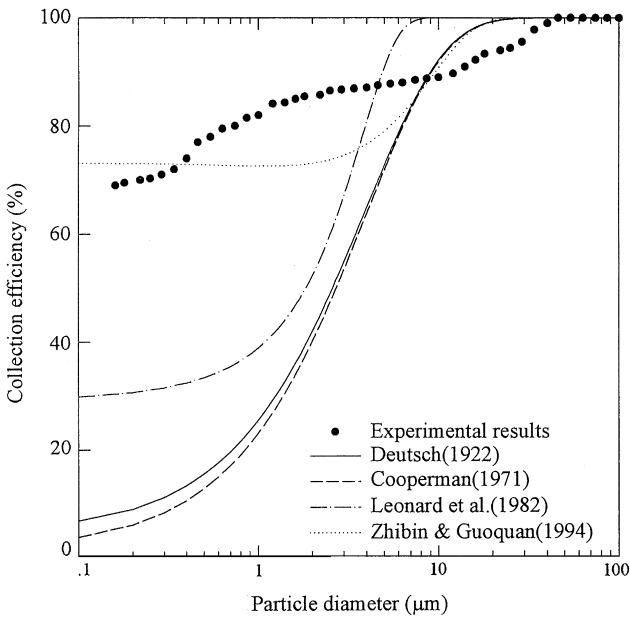
Fig. 11. Correlation of experimental result with other theoretical predictions of collection efficiency as a function of particle diameter. Experimental conditions: $V_w = 50$ kV, $S_x = 150$ mm, $S_y = 37.5$ mm, $U = 1$ m/s, $T_u = 12\%$.

Table 3
The optimum operating conditions of the present ESP experimental conditions

Dimensions and operating conditions	Values
Diameter of discharge wire, D_w (mm)	1
Wire-to-plate spacing, S_x (mm)	150
Wire-to-wire spacing, S_y (mm)	37.5
Length of collection plate, L (m)	0.75
Height of collection plate, H (m)	0.3
Air flow velocity, U (m/s)	1
Applied voltage on wires, V_w (kV)	50
Turbulence intensity, T_u (%)	15
Air temperature, T (K)	293
Air pressure, P (atm)	1

the fluid's turbulence level is decreased. It can also be observed that the turbulence affects somewhat the collection efficiency at the low electric field region. However, the collection efficiency at the high electric field region is not affected significantly. The diameter of the discharge wires also plays an important role for the ESP performance. As the wire diameter was increased as shown in Fig. 10, the collection efficiency is seen
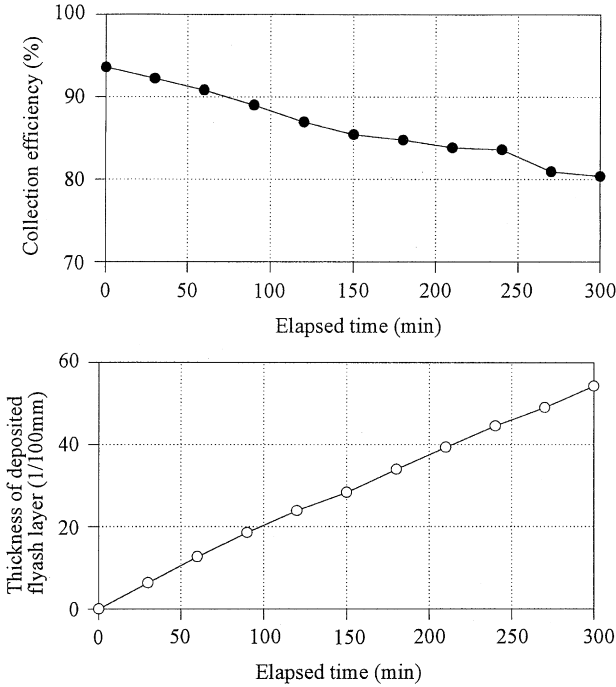
Fig. 12. Collection efficiency and thickness of deposited fly ash layer as a function of elapsed time. Experimental conditions: $D_w = 1$ mm, $S_x = 150$ mm, $S_y = 37.5$ mm, $V_w = 50$ kV, $U = 1$ m/s, $T_u = 12\%$.

to decrease. It is because an increase in the wire diameter leads to higher corona starting voltages and low electric field intensities at the surface of the wire at the corona onset. For a given applied voltage above the corona starting voltage, the corona will decrease as the wire diameter is increased. For the same average current density at the collection plate, the space charge density near the wire decreases as the corona wire diameter is increased. Thus, as the wire diameter is increased to maintain the average current density at the collection plate, it is necessary to increase the applied voltage. From these subsequent experiments, the optimum operating conditions which can give the highest particle collection efficiency of ESP are obtained as shown in Table 3. Fig. 11 shows comparison of the experimental results with the collection efficiency predicted by the models of Deutsch [1], Cooperman [2], Leonard et al. [3], and Zhibin and Guoquan [7]. This comparison shows that the collection efficiency measured is higher than that of all the used other models for the particle size range of 0.1–3 μm. Deutsch [1] and Cooperman [2] did not consider non-ideal parameters such as leakage, particle re-entrainment etc. Even though Leonard et al. [3] concentrated on the finite diffusivity, they could not predict successfully the behavior of small particles. Among the theories considered, the Zhibin and Guoquan [7] model which considered non-uniform gas velocity is again in relatively good agreement with the present experimental measurement results.
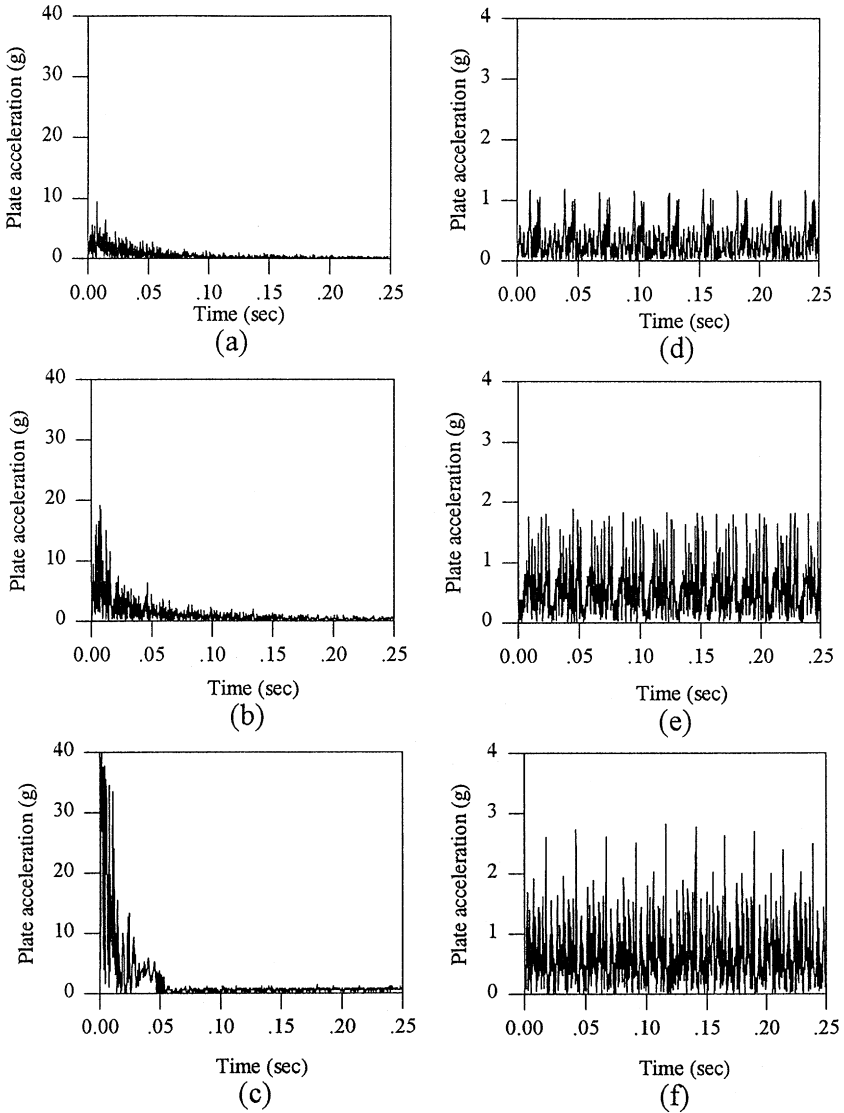
Fig. 13. Comparison of plate accelerations with various hammer and vibrator impactions ((a), (b), (c) Hammer swing angle; 45°, 60°, 90°, (d), (e), (f) vibrating steps; 6, 8, 10, respectively).

5. Rapping and particle re-entrainment

As time passes, the ESP performance tends to deteriorate due to particle accumulation on both the collection plates. It is because back corona takes place in the deposited dust layer. A back corona reduces the sparkover voltage and alters the nature of the coronas on the discharge electrodes. Thus, the back corona naturally
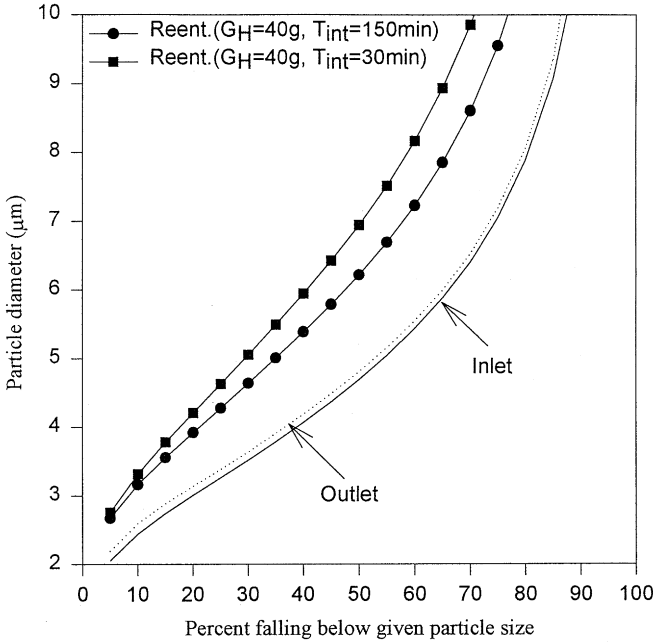
Fig. 14. Particle size distribution of inlet and outlet dusts for an ESP showing severe re-entrainment and agglomeration of the dust.

impairs performance of an electrostatic precipitator. Fig. 12 illustrates this phenomenon. After the elapsed time reaches 300 min, the collection efficiency is seen to have decreased to 80% from the initial efficiency of 95%. To study the effects of rapping, a rapping system equipped with two hammers plus a vibrator was designed and implemented [17,18]. During the rapping experiments, accelerations of the hammers, the vibrator, and the plates were measured using the dynamic signal analyzer and the accelerometer. The sensor was attached to the center of the collection plate. The hammer rapping system is limited to collecting electrode for cleaning of dry-type horizontal flow ESP [19]. The mechanism consists of a shaft running horizontally across the ESP between banks of collecting plates. The shaft is turned by hands. The hammers are connected to the shaft and then strike against the collecting plates. The rapping intensity was varied by adjusting the angle of the hammer swing. The hammers impacted the collection plate with a peak acceleration of 400–600 g, where g is a gravitational acceleration ($g = 9.8$ m/s^2). Depending on the angle of the hammer swing (45, 60, and 90°), the collection plates experienced a peak in-plane acceleration value, G_H (10g, 20g, and 40g) as in Fig. 13 [(a), (b), and (c), respectively]. In the case of vibrator, electromagnetic vibrators consisted of a balanced, spring-loaded armature suspended between two synchronized electro-magnetic coils. When energized, the armature vibrates at the line frequency. This vibrating energy is transmitted through a rod to the collection plates. In full scale ESPs, this device is used mainly in the
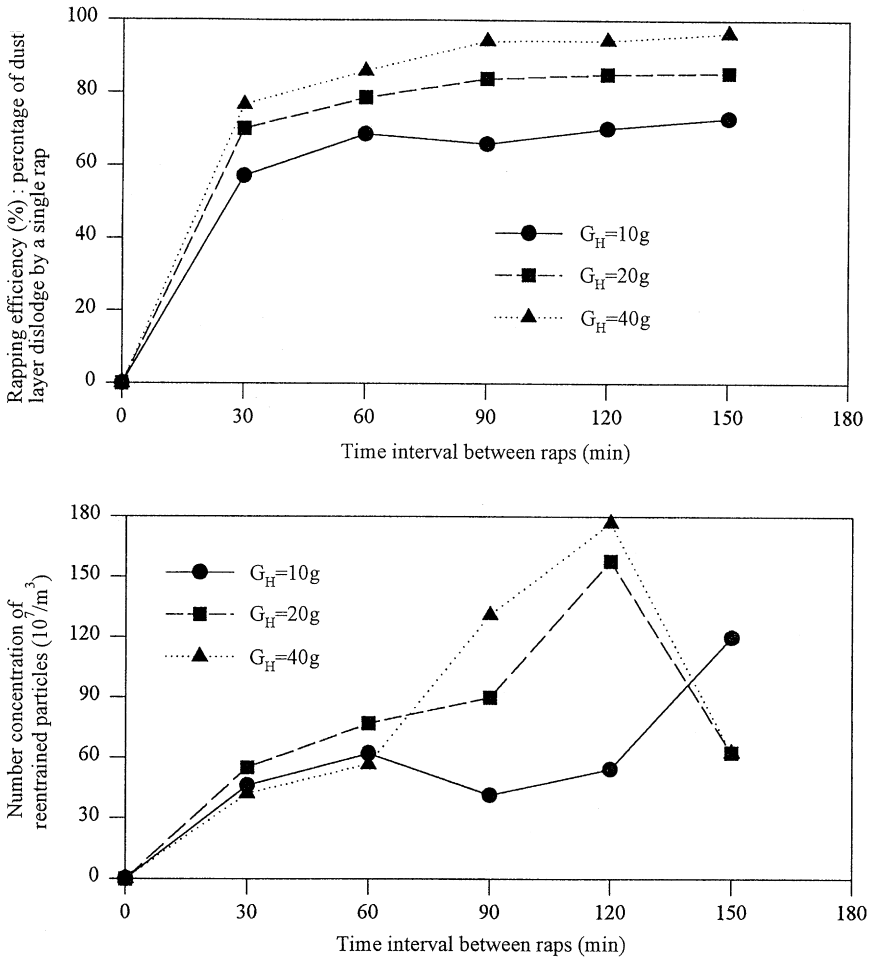
Fig. 15. Rapping efficiency and concentration of re-entrained particles as a function of time interval between raps (case: hammer rapping system).

vertical position for discharge electrode cleaning and for both horizontal and vertical flow dry-type ESP. The amplitude of vibration, operating time and frequency of vibration were controlled by varying the electrical energy input. Depending on the stage of vibrating (6 stage, 8 stage, and 10 stage), the collection plates had each peak acceleration value, G_V (1.2g, 2g, and 3g) as shown in Fig. 13 [(d), (e), and (f), respectively]. At first, the collection plates were impacted with hammers only. Here, the rapping efficiency was evaluated with the total mass of particles measured before and after rapping

$$\eta_{\text{rap}} = \frac{(m)_{\text{before}} - (m)_{\text{after}}}{(m)_{\text{before}}}, \tag{10}$$
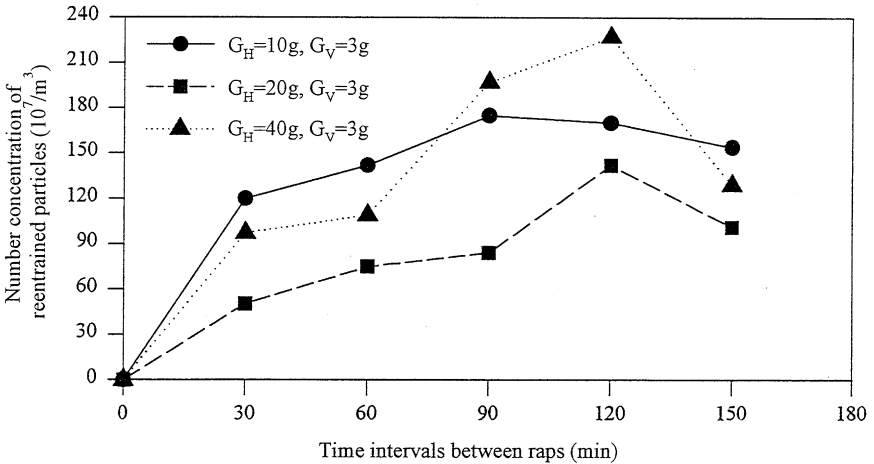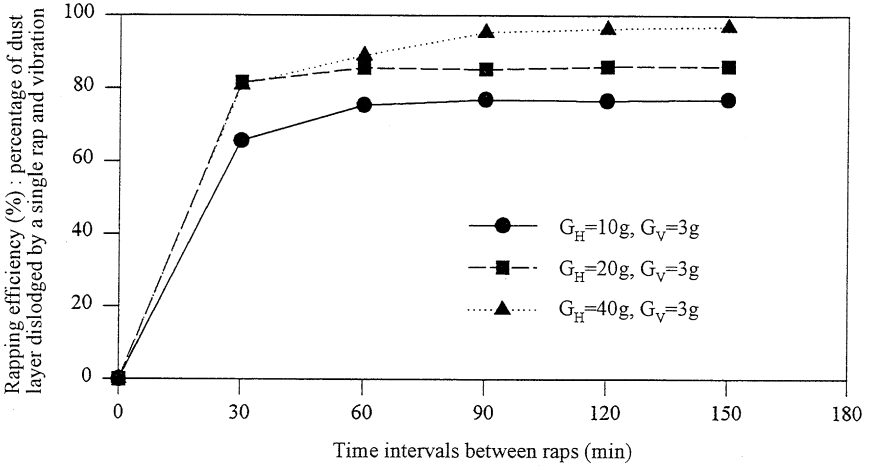
Fig. 16. Rapping efficiency and concentration of re-entrained particles as a function of time interval between raps (case: combined rapping system).

where $(m)_{before}$ is the total mass of deposited particles before rapping. $(m)_{after}$ is the total mass of deposited particles after rapping.

Concurrently, the particle size distribution was measured at the outlet of ESP to check the influence of the re-entrained particles. Fig. 14 shows that re-entrained particles are larger than the original particles. Obviously, the particles were aggregated to become compact during deposition. Fig. 15 shows that the rapping efficiency increased with increasing time interval between raps. It is because the thickness of deposited fly ash layer is increased. In other words, the aggregating force of deposited particles is sufficiently strong. Thus, if particles are impacted with shear force provided by the hammer, they would become separated from the collection
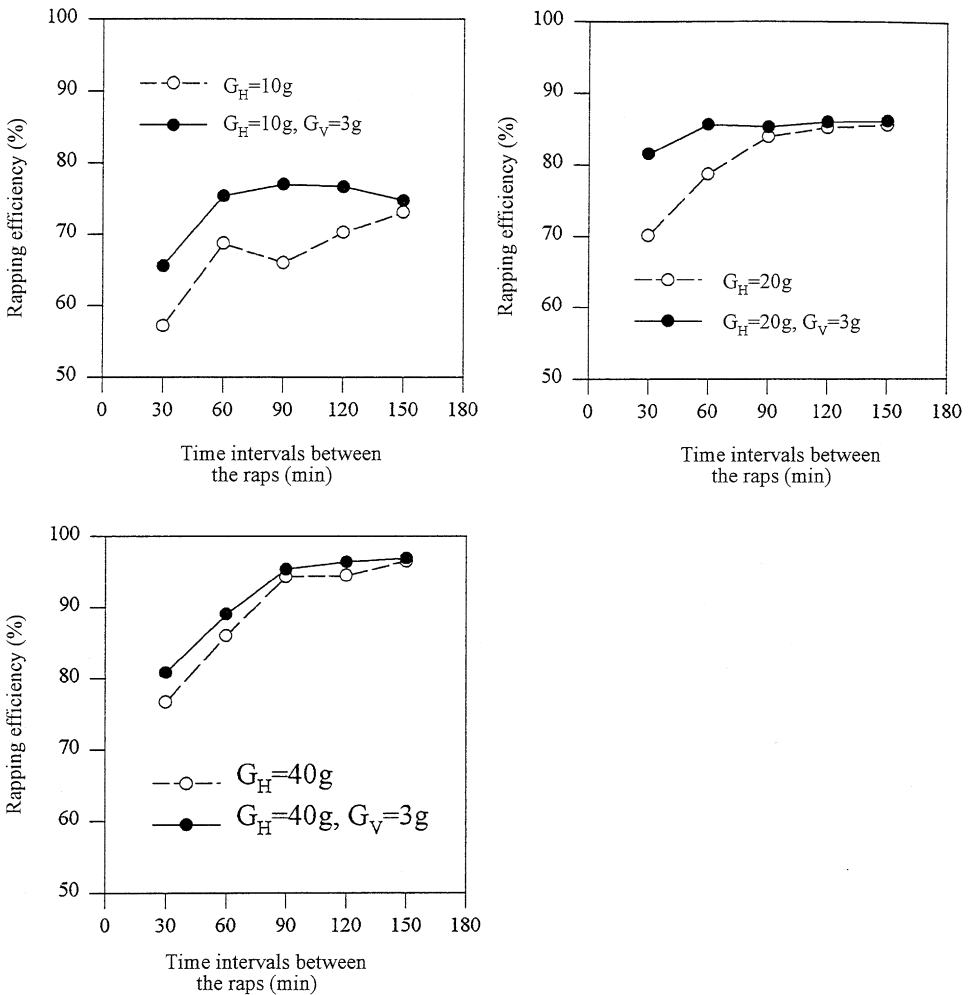
Fig. 17. Comparison of rapping efficiency of only hammer with that of hammer and vibrator rapping system as a function of time intervals between the raps.

plates and enter the hopper. The concentration of re-entrained particles increased with increasing rapping time interval after the maximum concentration was reached, the concentration starts decreasing rapidly. From these results, it can be predicted that thin dust layers are loosely held together and become disaggregated during rapping. Thus, thin layers produce fine aggregates that can be easily re-entrained, while thicker layers provide large aggregates that tend to fall into the hopper. As the second step, the collection plates were impacted with the hammer and the vibrator simultaneously (combined rapping system). Fig. 16 shows similar trend as Fig. 15. Subsequently, each result was compared in terms of the rapping efficiency and the concentration of re-entrained particles, respectively. Figs. 17 and 18 show that the
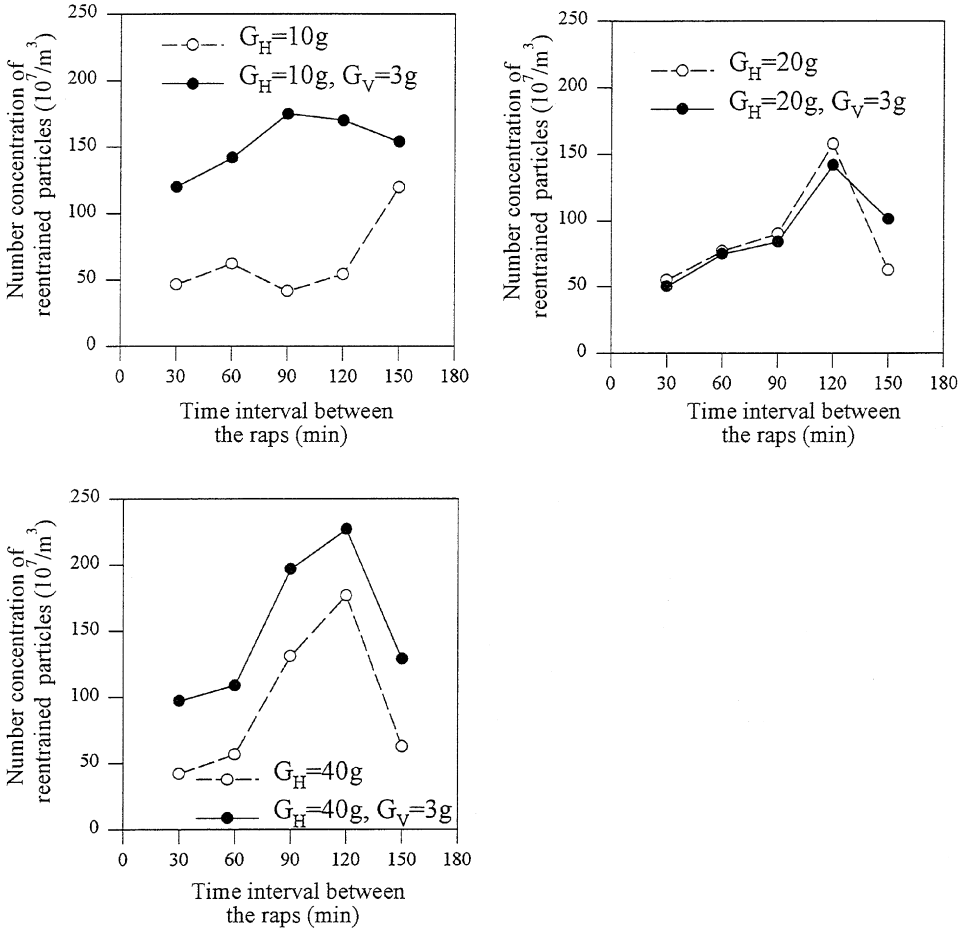
Fig. 18. Comparison of the concentration of re-entrained particles by only hammer rapping with that of re-entrained particles by combined rapping (hammer plus vibrator) as a function of time interval between the raps.

efficiency of the combined rapping is higher by 2–10% than that of the hammer rapping only. The concentration of re-entrained particles of combined rapping is generally much higher than that of only hammer rapping. From this result, it is found that unless the rapping system operates at a sufficiently high acceleration, only fine aggregates will be dislodged and re-entrained. Thus, this mechanism can adversely affect the performance of electrostatic precipitators. Finally, the optimum operating condition which had the combined rapping system ($G_H = 40g$, $G_V = 3g$) and the time interval between raps ($T_{int} = 150$ min) was applied to the ESP operating for 5 h and the change of the particle collection efficiency was measured. As seen in Fig. 19, the combined rapping system is recommended to keep the higher collection efficiency over a long elapsed operating time.
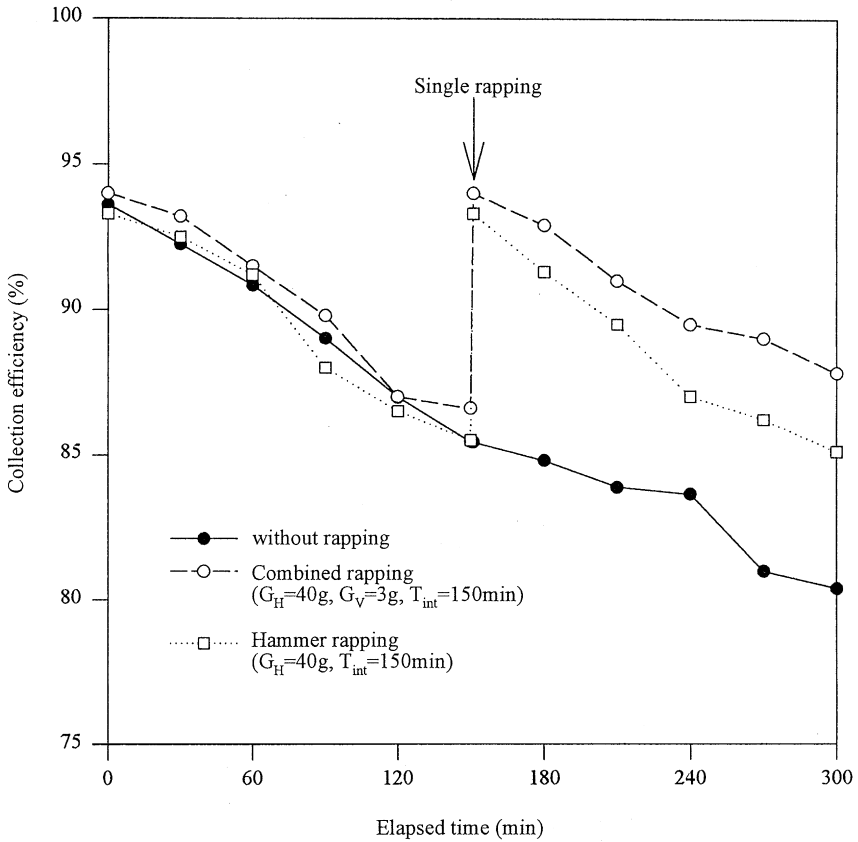
Fig. 19. Effect of rapping on collection efficiency as a function of elapsed time. Experimental conditions: $D_w = 1$ mm, $S_x = 150$ mm, $S_y = 37.5$ mm, $V_w = 50$ kV, $U = 1$ m/s, $T_u = 12\%$.

6. Conclusions

In this study, a laboratory-scale eight wire single-stage electrostatic precipitator was designed, built, and operated in a wind tunnel. At first, the optimum ESP operating conditions were sought for achieving relatively high collection efficiency. Secondly, characteristics of the rapping mechanisms were studied by varying different parameters including the thickness of fly ash layer, the magnitude of rapping acceleration, the hammer type and the vibrator type. As a result of the present experimental study, the following conclusions can be reached:

(1) As the diameter of discharging wires and the wire-to-plate spacing are decreased, a higher collection efficiency of ESP is obtained. For cases in which the wire-to-plate spacing is small ($S_x < 10$ mm), theoretical models predict much higher collection efficiency than experimentally measured efficiency. When the wire-to-plate spacing is large ($S_x > 15$ mm), the Deutsch [1] and the Cooperman [2]

models underestimate the collection efficiency compared to the experimental data. As the wire-to-plate spacing increased, the decreasing trend of experimental collection efficiency is similar to the model of Zhibin and Guoquan [7].

(2) In the multiwire single-stage ESP, there exists an optimum wire-to-wire spacing. In the present experiment, the highest collection efficiency occurred at $S_y = 37.5$ mm. Thus, the wire-to-wire spacing proves to be one of the important variables for achieving high collection efficiency with a multiwire single-stage ESP.

(3) As the air flow velocity increases, the overall particle collection efficiency decreases. Among the theories used, the Zhibin and Guoquan [7] model was found to be in a better agreement with the experimental data than the other models.

(4) Turbulence intensity before the precipitating region plays an important role in the low electric field region. However, in the high electric field region, particles deposit on the collection plates readily regardless of turbulence intensity.

(5) As the thickness of fly ash layer and the acceleration of rapping increase, the rapping efficiency increases. A combined rapping system consisting of hammer plus vibrator is recommended to maximize the rapping efficiency. Under the experimental conditions used in this study, a combination $G_H = 40g$ for hammer, $G_V = 3g$ for vibrator and a time interval between raps of $T_{int} = 150$ min, provided the highest rapping efficiency.

(6) With respect to particle re-entrainment, we confirmed that the number concentration of re-entrained particles increased with an increasing elapsed time. After reaching the maximum concentration, it decreases rapidly. This is in good agreement with the observations of Plato [20], Nichols et al. [21].

(7) The particles re-entrained during rapping are generally larger than original particles. Apparently, the size increase is due to the aggregating mechanism operating while particles remain deposited.

References

[1] W. Deutsch, Bewegung und Ladung der Elektrizitatstrager im Zylinderkondensator, Ann Phys. 68 (1922) 335–344.

[2] G. Cooperman, A new theory of precipitator efficiency, Atmos. Environ. 5 (1971) 541–551.

[3] G.L. Leonard, M. Mitchner, S.A. Self, Experimental study of the effect of turbulent diffusion on precipitator efficiency, J. Aerosol Sci. 13 (1982) 271–284.

[4] K.D. Khim, M. Mitchner, S.A. Self, Comparison of wire-plate and plate-plate electrostatic precipitators in turbulent flow, J. Electrostat. 19 (1987) 21–32.

[5] Z. Zhibin, Z. Guoquan, New model of electrostatic precipitation efficiency accounting for turbulent mixing, J. Aerosol Sci. 23 (2) (1992) 115–121.

[6] G.A. Kallio, D.E. Stock, Interaction of electrostatic and fluid dynamic fields in wire-plate electrostatic precipitators, J. Fluid Mech. 240 (1992) 133–166.

[7] Z. Zhibin, Z. Guoquan, Investigations of the collection efficiency of an electrostatic precipitator with turbulent effects, Aerosol Sci. Technol. 20 (1994) 169–176.

[8] H.J. White, Industrial Electrostatic Precipitation, Addison-Wesley, Reading, MA, 1963.

[9] N.A. Fuchs, On the stationary charge distribution on aerosol particles in a bipolar ionic atmosphere, Geofis. Pure Appl. 56 (1963) 185–193.

[10] K.H. Yoo et al., Charging and collection of submicron particles in two-stage parallel-plate electro-static precipitators, Aerosol Sci. Technol. 27 (1997) 308–323.

[11] G. Herdan, Small Particle Statics, 2nd ed., Academic Press, New York, 1980.

[12] W.T. Sproull, Minimizing rapping loss in precipitators at a 2000-megawatt coal-fired power station, J. Air Pollu. Control Assoc. 22 (3) (1972) 181–186.

[13] H.W. Spencer, Rapping re-entrainment in a nearly full scale pilot electrostatic precipitator, Environmental Protection Agency Publication, EPA-600/2-76-140, 1976.

[14] H.W. Spencer, Rapping re-entrainment in a nearly full scale pilot electrostatic precipitator, EPA-600/2-76-140, 1976.

[15] H.W. Spencer, D. Juricic, Electrostatic precipitator plate rapping and reliability, Joy Industrial Equipment Company, FP-1006, Vol. 3, Part 1, Los Angels, CA, 1980.

[16] O.J. Tassicker, Rapping re-entrainment losses in full-scale electrostatic precipitators, Conference and Course on Electrostatic Precipitation, Leura, NSW, Australia, 1978.

[17] J.R. McDonard, A.H. Dean, Electrostatic Precipitator Manual, Noyes Data Corporation, New Jersey, 1982.

[18] S. Oglesby, B. Grady, Electrostatic Precipitation, Marcel Dekker, New York, 1978.

[19] J.K. Lee et al., An experimental study of electrostatic precipitator plate rapping and re-entrainment, Proceedings of Seventh International Conference on Electrostatic Precipitation, Kyongju, Korea, 1998, pp. 155–162.

[20] H. Plato, Rapping of collecting plates in electrostatic precipitators, Staub-Reinhalt, Luft 29 (1969) 22–30 (in English).

[21] G.B. Nichols, H.W. Spencer, J.D. McCain, Rapping re-entrainment study, Report to Tennessee Valley Authority, TVA Agreement TV36921A, November 1975.